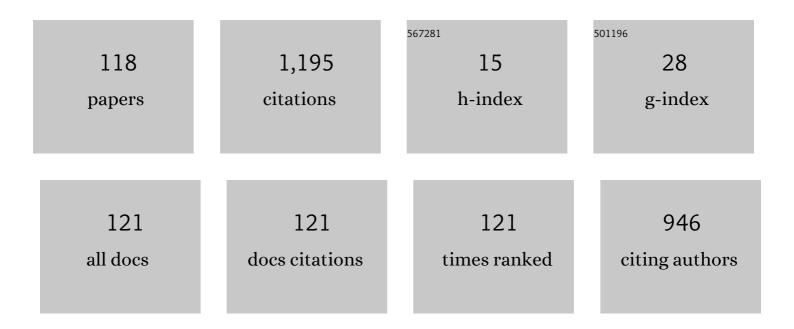
List of Publications by Year in descending order

Source: https://exaly.com/author-pdf/1559735/publications.pdf Version: 2024-02-01



SHIPO KUBUKI

#	Article	IF	CITATIONS
1	Structural Characterization of Gel-Derived Calcium Silicate Systems. Journal of Physical Chemistry A, 2010, 114, 10403-10411.	2.5	87
2	Elucidating the Mechanistic Origin of a Spin State-Dependent FeN _{<i>x</i>} –C Catalyst toward Organic Contaminant Oxidation via Peroxymonosulfate Activation. Environmental Science & Technology, 2022, 56, 1321-1330.	10.0	81
3	Non-HPLC Rapid Separation of Metallofullerenes and Empty Cages with TiCl ₄ Lewis Acid. Journal of the American Chemical Society, 2012, 134, 9762-9767.	13.7	70
4	PVP surfactant-modified flower-like BiOBr with tunable bandgap structure for efficient photocatalytic decontamination of pollutants. Applied Surface Science, 2020, 530, 147233.	6.1	67
5	BiOBr/MoS2 catalyst as heterogenous peroxymonosulfate activator toward organic pollutant removal: Energy band alignment and mechanism insight. Journal of Colloid and Interface Science, 2021, 594, 635-649.	9.4	51
6	Self-Assembly of Nanosheet-Supported Fe-MOF Heterocrystals as a Reusable Catalyst for Boosting Advanced Oxidation Performance via Radical and Nonradical Pathways. ACS Applied Materials & Interfaces, 2021, 13, 22694-22707.	8.0	40
7	The formation and microstructural properties of uniform α-GaOOH particles and their calcination products. Journal of Alloys and Compounds, 2015, 620, 217-227.	5.5	38
8	Occupation of tungsten site by iron in sodium tungstate glasses. Journal of Non-Crystalline Solids, 1996, 194, 23-33.	3.1	30
9	Influence of Fe(III) doping on the crystal structure and properties of hydrothermally prepared β-Ni(OH)2 nanostructures. Journal of Alloys and Compounds, 2018, 750, 687-695.	5.5	30
10	Crystallization mechanism of aluminoferrate glass accompanying a precipitation of nanocrystals of dicalcium ferrite (Ca2Fe2O5) and mayenite (12CaO·7Al2O3). Journal of Materials Chemistry, 1997, 7, 1801-1806.	6.7	29
11	Synthesis and properties of indium-doped hematite. Journal of Alloys and Compounds, 2017, 695, 1900-1907.	5.5	27
12	Crystallization and Structural Relaxation of xBaO (90-x)V2O5 10Fe2O3 Glasses Accompanying an Enhancement of the Elctric Conductivity. Journal of the Ceramic Society of Japan, 2007, 115, 776-779.	1.1	23
13	Self-assembly of MoS2 nanosheet adhered on Fe-MOF heterocrystals for peroxymonosulfate activation via interfacial interaction. Journal of Colloid and Interface Science, 2022, 608, 3098-3110.	9.4	22
14	57Fe and 119Sn Mössbauer, XRD, FTIR and DC conductivity study of Li2O Fe2O3SnO2P2O5 glass and glass ceramics. Journal of Alloys and Compounds, 2018, 765, 121-127.	5.5	18
15	Synthesis and microstructural properties of mixed iron–gallium oxides. Journal of Alloys and Compounds, 2015, 634, 130-141.	5.5	17
16	Structural Study of Glass and Glass Ceramics Prepared with Egyptian Basalt. Silicon, 2015, 7, 383-391.	3.3	16
17	Photo-Fenton degradation of methylene blue using hematite-enriched slag under visible light. Journal of Radioanalytical and Nuclear Chemistry, 2020, 325, 537-549.	1.5	16
18	Influence of Cr doping on the structural, magnetic, optical and photocatalytic properties of α-Fe2O3 nanorods. Journal of Physics and Chemistry of Solids, 2021, 148, 109699.	4.0	16

#	Article	IF	CITATIONS
19	Synthesis, characterization and magnetic properties of ε-Fe2O3 nanoparticles prepared by sol-gel method. Journal of Magnetism and Magnetic Materials, 2021, 538, 168264.	2.3	16
20	Solidification of Hazardous Heavy Metal Ions with Soda-Lime Glass. Characterization of Iron and Zinc in the Waste Glass Journal of the Ceramic Society of Japan, 2000, 108, 245-248.	1.3	15
21	M^ ^ouml;ssbauer Study of Water-Resistive Conductive Vanadate Glass. Radioisotopes, 2012, 61, 463-468.	0.2	15
22	Visible light activated photo-catalytic effect and local structure of iron silicate glass prepared by sol-gel method. Hyperfine Interactions, 2014, 226, 747-753.	0.5	13
23	Visible-light activated photocatalytic effect of glass and glass ceramic prepared by recycling waste slag with hematite. Pure and Applied Chemistry, 2017, 89, 535-544.	1.9	13
24	Structural, electrical and photocatalytic properties of iron-containing soda-lime aluminosilicate glass and glass-ceramics. Journal of Non-Crystalline Solids, 2021, 553, 120510.	3.1	13
25	Characterization and Conduction Mechanism of Highly Conductive Vanadate Glass. Croatica Chemica Acta, 2015, 88, 427-435.	0.4	13
26	Enhancement of electrical conductivity and chemical durability of 20R2O•10Fe2O3•xWO3•(70â^'x)V2O5 glass (R=Na, K) caused by structural relaxation. Journal of Non-Crystalline Solids, 2013, 378, 227-233.	3.1	12
27	Visible light activated catalytic effect of iron containing soda-lime silicate glass characterized by 57Fe-MA¶ssbauer spectroscopy. Journal of Radioanalytical and Nuclear Chemistry, 2014, 301, 1-7.	1.5	12
28	Photo-Fenton catalytic ability of iron-containing aluminosilicate glass prepared by sol-gel method. Journal of Alloys and Compounds, 2020, 816, 153227.	5.5	12
29	Influence of low-spin Co3+ for high-spin Fe3+ substitution on the structural, magnetic, optical and catalytic properties of hematite (I±-Fe2O3) nanorods. Journal of Physics and Chemistry of Solids, 2021, 152, 109929.	4.0	12
30	Structural characterization, electrical and photocatalytic properties of αâ^'and γ-Fe2O3 nanoparticles dispersed in iron aluminosilicate glass. Journal of Non-Crystalline Solids, 2021, 561, 120756.	3.1	12
31	IR transmission method applied to the crystallization of gallate glasses and the mechanism of crystallization caused by Ar+ laser and 60Co γ-ray irradiation. Journal of Non-Crystalline Solids, 1994, 177, 193-199.	3.1	11
32	Mössbauer study of semiconducting and ferrimagnetic fly ash-recycled glass. Journal of Radioanalytical and Nuclear Chemistry, 2005, 266, 171-177.	1.5	11
33	Incorporation of Fe in the interlayer of Na-bentonite <i>via</i> treatment with FeCl ₃ in acetone. Clays and Clay Minerals, 2007, 55, 89-95.	1.3	11
34	Electrical conductivity and local structure of barium manganese iron vanadate glass. Hyperfine Interactions, 2012, 207, 61-65.	0.5	11
35	Structural analysis and visible light-activated photocatalytic activity of iron-containing soda lime aluminosilicate glass. Journal of Alloys and Compounds, 2015, 645, 1-6.	5.5	11
36	The effects of In 3+ doping on the properties of precipitated goethite. Journal of Alloys and Compounds, 2016, 658, 41-48.	5.5	11

#	Article	IF	CITATIONS
37	Highly conductive barium iron vanadate glass containing different metal oxides. Pure and Applied Chemistry, 2017, 89, 419-428.	1.9	10
38	57Fe-Mössbauer study and methylene blue decomposing effect of nanoparticle mixtures composed of metallic iron and maghemite. Journal of Alloys and Compounds, 2017, 722, 94-100.	5.5	9
39	The relationship between local structure and photo-Fenton catalytic ability of glasses and glass-ceramics prepared from Japanese slag. Journal of Radioanalytical and Nuclear Chemistry, 2019, 322, 751-761.	1.5	9
40	57Fe-Mössbauer and XAFS Studies of Conductive Sodium Phospho-Vanadate Glass as a Cathode Active Material for Na-ion Batteries with Large Capacity. Journal of Non-Crystalline Solids, 2021, 570, 120998.	3.1	9
41	Characterization of electrically conductive vanadate glass containing tungsten oxide. Journal of Radioanalytical and Nuclear Chemistry, 2013, 295, 1123-1128.	1.5	8
42	Various Three-Dimensional Structures Connected by Al–O/OH/Acetate–Al Bonds. Inorganic Chemistry, 2013, 52, 13238-13243.	4.0	8
43	57Fe-Mössbauer study of electrically conductive alkaline iron vanadate glasses. Journal of Radioanalytical and Nuclear Chemistry, 2014, 299, 453-459.	1.5	8
44	Photocatalytic degradation of organic dyes and phenol by iron-silicate glass prepared by the sol–gel method. New Journal of Chemistry, 2021, 45, 19019-19031.	2.8	8
45	Application of the "Tg-Δ rule―to the local structural study of ferrate glasses. Journal of Radioanalytical and Nuclear Chemistry, 1999, 239, 237-240.	1.5	7
46	'TgDELTA. Rule' Applied to Semiconducting Vanadate Glasses Containing Different Amounts of Fe2O3 Journal of the Ceramic Society of Japan, 1999, 107, 408-412.	1.3	7
47	Mössbauer study of FINEMET with different permeability. Hyperfine Interactions, 2013, 219, 63-67.	0.5	7
48	Mössbauer study of novel iron(II)-dioxime complexes with branched alkyl chains. Hyperfine Interactions, 2014, 226, 181-185.	0.5	7
49	Corelationship between local structure and water purifying ability of iron-containing waste glasses. Hyperfine Interactions, 2006, 166, 429-436.	0.5	6
50	Electrical conductivity and local structure of lithium tin iron vanadate glass. Hyperfine Interactions, 2013, 219, 141-145.	0.5	6
51	Water cleaning ability and local structure of iron-containing soda-lime silicate glass. Hyperfine Interactions, 2013, 218, 41-45.	0.5	6
52	Decomposition mechanism of methylene blue caused by metallic iron-maghemite mixture. Hyperfine Interactions, 2013, 218, 47-52.	0.5	6
53	Effect of the structural change of an iron–iron oxide mixture on the decomposition of trichloroethylene. Journal of Radioanalytical and Nuclear Chemistry, 2013, 295, 23-30.	1.5	6
54	A relationship between oxidation state of iron and color of Arita celadon glaze characterized by ⁵⁷ Fe-Mössbauer spectroscopy. Journal of the Ceramic Society of Japan, 2014, 122, 520-522.	1.1	6

#	Article	IF	CITATIONS
55	Effect of phosphorus precursors on the structure of bioactive calcium phosphate silicate systems. Materials Science and Engineering C, 2017, 73, 767-777.	7.3	6
56	Effect of Substitutional Doping of Tin in Highly Conductive Barium Iron Vanadate Glass. Physica Status Solidi (A) Applications and Materials Science, 2018, 216, 1800157.	1.8	6
57	Application of the IR transmission method and the Mössbauer effect to the crystallization of calcium gallate glass. Journal of Non-Crystalline Solids, 1997, 209, 87-95.	3.1	5
58	Mössbauer study on the crystallization of IR-transmitting aluminate glasses. Journal of Radioanalytical and Nuclear Chemistry, 1999, 239, 303-307.	1.5	5
59	Effect of FeCl3 and acetone on the structure of Na–montmorillonite studied by Mössbauer and XRD measurements. Hyperfine Interactions, 2006, 166, 643-649.	0.5	5
60	Mössbauer study of new vanadate glass with large charge-discharge capacity. Hyperfine Interactions, 2014, 226, 765-770.	0.5	5
61	A relationship between electrical conductivity and structural relaxation of 10SnO ₂ ·10Fe ₂ 0 ₃ ∣	dot;10P8 1.1	lt;sub>28
62	Waste water purification using new porous ceramics prepared by recycling waste glass and bamboo charcoal. Applied Water Science, 2017, 7, 4281-4286.	5.6	5
63	Structural characterization and magnetic properties of iron-phosphate glass prepared by sol-gel method. Journal of Non-Crystalline Solids, 2020, 543, 120158.	3.1	5
64	Local structure, glass transition, structural relaxation, and crystallization of functional oxide glasses investigated by MA¶ssbauer spectroscopy and DTA. Journal of Materials Science: Materials in Electronics, 2021, 32, 23655-23689.	2.2	5
65	Title is missing!. Journal of Radioanalytical and Nuclear Chemistry, 2000, 246, 43-49.	1.5	4
66	Propriedades estruturais e eletrônicas de óxidos de ferro em esmaltes celadon (II). Ceramica, 2012, 58, 534-541.	0.8	4
67	Mössbauer study of conductive oxide glass. AIP Conference Proceedings, 2014, , .	0.4	4
68	Mössbauer study of pH dependence of iron-intercalation in montmorillonite. Hyperfine Interactions, 2016, 237, 1.	0.5	4
69	Structural relaxation and electrical conductivity of molybdovanadate glass. Journal of Materials Science: Materials in Electronics, 2018, 29, 2654-2659.	2.2	4
70	Mössbauer and photocatalytic studies of CaFe2O4 nanoparticle-containing aluminosilicate prepared from domestic waste simulated slag. Journal of Radioanalytical and Nuclear Chemistry, 2019, 322, 1469-1476.	1.5	4
71	119Sn and 57Fe MÓ§ssbauer study of highly conductive vanadate glass. Journal of Materials Science: Materials in Electronics, 2019, 30, 8847-8854.	2.2	4
72	Municipal waste slag for dyes photocatalytic and metal recovery applications through structural analysis and experimental characterization. International Journal of Energy Research, 2021, 45, 17691-17708.	4.5	4

#	Article	IF	CITATIONS
73	Role of Sulfur as a Reducing Agent for the Transition Metals Incorporated into Lithium Silicate Glass. Croatica Chemica Acta, 2015, 88, 505-510.	0.4	4
74	Development of electrically conductive ZrO2-CaO-Fe2O3-V2O5 glass and glass-ceramics as a new cathode active material for Na-ion batteries with high performance. Journal of Alloys and Compounds, 2022, 899, 163309.	5.5	4
75	Highly covalent Felll–O bonding in photo-Fenton active Sn-doped goethite nanoparticles. Materials Chemistry and Physics, 2022, 287, 126247.	4.0	4
76	Mössbauer study of oxygen adducts in solid Fe(II) phthalocyanines. Journal of Physics: Conference Series, 2010, 217, 012029.	0.4	3
77	Electrical conductivity and local structure of iron-containing lithium barium vanadate glass. Journal of Physics: Conference Series, 2010, 217, 012026.	0.4	3
78	Mössbauer study of metallic iron and iron oxide nanoparticles having environmental purifying ability. , 2014, , .		3
79	Photocatalytic effect and Mössbauer study of iron titanium silicate glass prepared by sol-gel method. Hyperfine Interactions, 2015, 232, 51-58.	0.5	3
80	The relationship between SnII fraction and visible light activated photocatalytic activity of SnOx·SiO2 glass studied by Mössbauer spectroscopy. Journal of Radioanalytical and Nuclear Chemistry, 2017, 311, 1859-1865.	1.5	3
81	Magnetic property and 57Fe Mössbauer analysis of dilute Fe and Nb codoped SrTiO3-Π(STO) perovskites. Hyperfine Interactions, 2020, 241, 1.	0.5	3
82	Electrical Transport in Iron Phosphate-Based Glass-(Ceramics): Insights into the Role of B2O3 and HfO2 from Model-Free Scaling Procedures. Nanomaterials, 2022, 12, 639.	4.1	3
83	Laser- and gamma-ray induced crystallization of IR-transmitting calcium gallate glass. Hyperfine Interactions, 1994, 94, 2125-2130.	0.5	2
84	Substitution of Fe(III) for Ga(III) in calcium gallate glass confirmed from the Debye temperature. Journal of Radioanalytical and Nuclear Chemistry, 1998, 237, 47-50.	1.5	2
85	Title is missing!. Journal of Radioanalytical and Nuclear Chemistry, 2000, 246, 51-56.	1.5	2
86	Dissolution behaviour of iron silicate glass. Hyperfine Interactions, 2009, 192, 31-36.	0.5	2
87	Local structures and electronic band states of αâ^'Fe2O3 polycrystalline particles in the glazes of the HIZEN celadons produced in the Edo period of Japan, by means of X-ray absorption spectra (II). Ceramica, 2011, 57, 155-165.	0.8	2
88	[sup 57]Fe MoÌ^ssbauer study of iron-containing soda-lime silicate glass with COD reducing ability. , 2012, , .		2
89	Controlled crystallization a ionic conductivity of nanostructured LiNbFePO 4 glass ceramic. Hyperfine Interactions, 2014, 226, 131-140.	0.5	2
90	Emergence of ferromagnetism due to charge transfer in compressed ilmenite powder using super-high-energy ball milling. Scientific Reports, 2020, 10, 5293.	3.3	2

#	Article	IF	CITATIONS
91	Structural characterization and visible light activated photocatalytic ability of glass–ceramics prepared from municipal solid waste. Journal of Material Cycles and Waste Management, 2021, 23, 2266-2277.	3.0	2
92	A Mossbauer Study of the Low Spin-High Spin Transition of an Oxygen Adduct Formed in Solid β -Fe(II)Phthalocyanine. Open Inorganic Chemistry Journal, 2008, 2, 69-72.	0.3	2
93	Corelationship between local structure and water purifying ability of iron-containing waste glasses. , 2006, , 429-436.		2
94	Mössbauer study of some novel iron-bis-glyoxime and iron-tris-glyoxime complexes. Hyperfine Interactions, 2022, 243, 1.	0.5	2
95	Reduction of iron(III) in annealed asbestos/chrysotile. Hyperfine Interactions, 2008, 186, 161-166.	0.5	1
96	Mechanical strength and local structure of 'new' Hagi porcelain investigated by ⁵⁷ Fe-Mössbauer spectroscopy. Journal of Physics: Conference Series, 2010, 217, 012067.	0.4	1
97	[sup 57]Fe Mol̀^ssbauer study of conductive vanadate glass with high chemical durability. AIP Conference Proceedings, 2012, , .	0.4	1
98	Reclassification of CK chondrites confirmed by elemental analysis and Fe-Mössbauer spectroscopy. Hyperfine Interactions, 2012, 208, 75-78.	0.5	1
99	Mechanically strengthened new Hagi porcelain developed by controlling the chemical environment of iron. Hyperfine Interactions, 2012, 211, 173-180.	0.5	1
100	Degradation of Trichloroethylene and Methylene Blue by a Mixture of FeO and γ-Fe2O3 â^' A Review. ACS Symposium Series, 2014, , 179-191.	0.5	1
101	Magnetic interaction in oxygenated alpha Fe-phthalocyanines. , 2014, , .		1
102	Visible Light-Activated Photocatalytic Effect of Iron-Containing Silicate Glass - A Review. ACS Symposium Series, 2014, , 71-84.	0.5	1
103	Local structure and water cleaning ability of iron oxide nanoparticles prepared by hydro-thermal reaction. Hyperfine Interactions, 2014, 226, 489-497.	0.5	1
104	Determination of iron species, including biomineralized jarosite, in the iron-hyperaccumulator moss Scopelophila ligulata by M¶ssbauer, X-ray diffraction, and elemental analyses. BioMetals, 2019, 32, 171-184.	4.1	1
105	'Ea-δrule' applied to the crystallization study of gallate and vanadate glasses. Journal of Radioanalytical and Nuclear Chemistry, 2005, 266, 527-532.	1.5	0
106	57Fe-Mössbauer study of electrically conducting barium iron vanadate glass after heat treatment. Hyperfine Interactions, 2008, 185, 115-121.	0.5	0
107	Effect of nanocrystallization on the electrical conduction of silver lithium phosphate glasses containing iron and vanadium. Hyperfine Interactions, 2012, 205, 91-95.	0.5	0
108	Structural Characterization of Electrical Conductive Vanadate Glass. Radioisotopes, 2014, 63, 117-117.	0.2	0

#	Article	IF	CITATIONS
109	Electrical conductivity and local structure of lithium iron tungsten vanadate glass. Hyperfine Interactions, 2014, 226, 755-763.	0.5	0
110	B23-P-20The STEM Study of Crystalized Iron Vanadate Glasses Containing Alkaline Earth Oxide. Microscopy (Oxford, England), 2015, 64, i121.2-i121.	1.5	0
111	Synthesis of 14C labeled C60 with higher specific radioactivity. Journal of Radioanalytical and Nuclear Chemistry, 2015, 303, 1233-1237.	1.5	Ο
112	Improving the visible-light photocatalytic activity of SnOx·SiO2 glass systems by introducing SnOx nanoparticles. Journal of Radioanalytical and Nuclear Chemistry, 2018, 316, 579-586.	1.5	0
113	State analysis of fluorine-doped SnO2 (FTO) by 57Fe Mössbauer spectroscopy. Hyperfine Interactions, 2019, 240, 1.	0.5	0
114	Dissolution behaviour of iron silicate glass. , 2009, , 533-538.		0
115	Water cleaning ability and local structure of iron-containing soda-lime silicate glass. , 2012, , 197-201.		Ο
116	Decomposition mechanism of methylene blue caused by metallic iron-maghemite mixture. , 2012, , 203-208.		0
117	Electrical conductivity and local structure of lithium tin iron vanadate glass. , 2012, , 459-463.		0
118	Structural Characterization of Electrical Conductive Vanadate Glass. Radioisotopes, 2014, 63, 69-77.	0.2	0